ORNL/CP-100102

Evaluation of Margins in the ASME Rules for Defining the P-T Curve for a RPV

T. L. Dickson, W. J. McAfee, W. E. Pennell, and P. T. Williams
Oak Ridge National Laboratory

Abstract

The pressure-temperature (P-T) curve controls the upper-bound to the permissible operating envelope for a reactor pressure vessel (RPV) during the normal start-up and cool-down transients. The P-T operating envelope is progressively restricted because of irradiation embrittlement of the RPV material. In recent years, a number of electric utility companies have reported that the plant-specific P-T operating envelope has become so restricted that operation of the reactor during the heat-up and cool-down transients has become very difficult. An evaluation of the inherent margins in the current American Society of Mechanical Engineers (ASME) Code P-T curve rules was made to determine if they can be modified so as to increase the available P-T operating envelope while retaining adequate safety factors. The evaluation was made in the U. S. Nuclear Regulatory Commission (USNRC)-funded Heavy Section Steel Technology (HSST) program at Oak Ridge National Laboratory (ORNL) using results from a number of NRC-funded research programs. Best estimate allowable pressure (P_{BE}) calculations included all loading conditions and crack-front locations with the safety factor on pressure loading set to 1.0. The P_{BE} value obtained when the material fracture toughness was set at the lower-bound to the shallow-flaw database for RPV materials was higher than the allowable pressure obtained when K_{Ia} is replaced by K_{Ic} in the P-T curve rules. This finding supports opening of the P-T operation envelope by using K_{Ic} instead of K_{Ia} in the ASME P-T curve rules. It is important to recognize, however, that lower-bound to the shallow-flaw fracture toughness database is controlled by results from clad cruciform biaxial-loading tests conducted at normalized temperatures ($T\text{-}RT_{NDT}$) not less than -40°F. A potential exists for the estimated shallow-flaw lower-bound fracture toughness to be further adjusted if data from clad cruciform biaxial-loading tests become available for the normalized temperature range $-200°F \leq T\text{-}RT_{NDT} \leq -170°F$.

1. Introduction

Principal features of the RPV P-T operating envelope are shown in Fig. 1. The upper-bound to the P-T envelope is defined by the vessel material P-T curve [1], modified by the operating characteristics of the low temperature overpressure protection (LTOP) system required by the USNRC Standard Review Plan

DISCLAIMER

[2]. The lower-bound of the P-T operating envelope is set by the pressure required at a given temperature to prevent cavitation of the main coolant pumps, and/or activate the pump seals. Adjustment of the P-T curve to accommodate the effects of irradiation embrittlement of the RPV material results in a severe restriction of the P-T operating envelope. A concern exists that the potential for operator errors and opening of relief valves is greater when the operating envelope is severely restricted. This concern led to an investigation to determine if a basis exists for opening-up the P-T operating envelope while preserving essential RPV safety margins. The specific objective for the investigation was to determine if margins in the P-T curve analysis procedures were sufficient to support the substitution of the ASME K_{Ic} curve in place of the K_{Ia} curve in the analysis procedures of Ref. 1. The allowable pressure determined using this substitution is designated $P_{NEWCODE}$. The approach taken in the P-T curve margin study was to use best estimate data from RPV structural integrity research programs as input to calculate a best estimate allowable pressure P_{BE}. Demonstration of margins sufficient to justify the proposed ASME Code change requires that $P_{BE} \geq P_{NEWCODE}$.

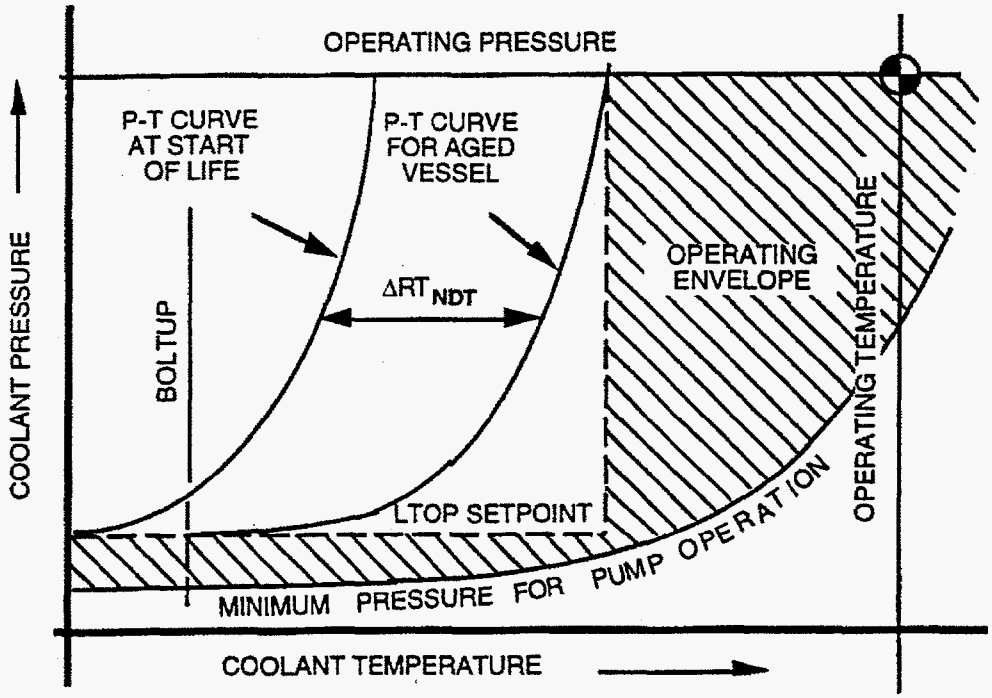

Fig. 1 The P-T operating envelope for a RPV is progressively restricted because of adjustment of the P-T curve to accommodate the effects of irradiation embrittlement of the RPV material.

2. P-T Curve Margin Assessment Rationale, Method and Scope

2.1 Rationale

Fracture technology research conducted since the P-T curve rules of Ref. 1 were formulated has identified a number of areas where those rules include unnecessary levels of conservatism, and some areas where

the level of conservatism was less than had been anticipated. Examples of unnecessary conservatism include the use in the P-T curve analyses of, (a) the lower-bound (K_{Ia}) crack arrest fracture toughness curve, and (b) a conservative inner surface flaw, having a depth corresponding to 25% of the RPV wall thickness (1/4t). Use of the K_{IR} curve reflects an early concern [3] that fracture could originate from local brittle zones in the RPV as a pop-in and propagate in a dynamic manner to the 1/4t depth. Fracture toughness tests on irradiated weld material, however, showed that data from specimens which had pop-ins fell within the scatter band of data from specimens which failed with no prior pop-ins [4]. Use of the K_{Ia} curve to safeguard against failure initiating from a local brittle zone was shown to be unnecessary.

Specification of the 1/4t flaw depth was made in 1972, when data on flaw-size-distribution and flaw density in RPV's were scarce [3]. At the time it was specified, the 1/4t flaw was considered to be very conservative. Since that time, data from non-destructive examinations (NDE's) of a significant number of "LWR vessels, made essentially to ASME III rules alone," have been published [5]. While a number of flaws in the size range $0.5" \leq a \leq 1.0"$ were reported, no flaws with a radial depth greater than 1.0" were found. A similar finding was obtained from the recently completed NDE and destructive examination, conducted by Dr. S. Doctor of Pacific Northwest National Laboratory, on the RPV from the Pressure Vessel Research User's Facility at ORNL [6]. Results from these investigations support the use of a 1" deep flaw in the P_{BE} evaluations.

The rules of Ref. 1, and the sample problem defined later in this paper, both define a 6:1 aspect ratio surface-breaking flaw. A check was made in this evaluation to determine if the assumption of a surface-breaking flaw introduced an element of unnecessary conservatism. Any significant flaws in the inner surface structural material of a RPV (plate, forging, and weld) would be introduced during fabrication operations, which would have been completed before the application of stainless steel cladding to the inside surface of the RPV. A surface-breaking flaw, which existed in the inside surface of the RPV prior to cladding, would be converted to a sub-clad flaw by the cladding process. Stress intensity factors induced by P-T loading on a sub-clad flaw would be substantially lower than those induced in a surface-breaking flaw by the same loading. Cleavage-controlled allowable pressures for a subclad flaw could, therefore, be significantly higher than the allowable pressures for a surface-breaking flaw. For P-T curve margins based on a subclad flaw to be valid, however, it must be shown that the cladding above the flaw remains integral throughout the operating life of the RPV. An investigation of the structural integrity of the cladding above a sub-clad flaw, based on both tensile instability and ductile tearing failure modes, was included in this P-T curve margin assessment.

2.2 Method

The P-T curve analysis rules of Ref. 1 use the following equation to define the P-T curve for a RPV. K_{Im} values are determined using conditions at the deepest point on the flaw and the applied stress intensity factors (K_{Im} and K_{It}) are determined at the same location.

$$2K_{Im} + K_{It} < K_{Ia} \qquad (1)$$

Where:

K_{Im} is the stress intensity factor produced by pressure-induced membrane loading in the RPV shell (ksi$\sqrt{}$in.).

K_{It} is the stress intensity factor produced by a radial thermal gradient through the wall of the RPV (ksi$\sqrt{}$in.).

K_{Ia} is the lower bound stress intensity factor obtained from crack-arrest tests (ksi$\sqrt{}$in.).

The factor of two applied to K_{Im} in equation 1 is the means by which allowance is made to accommodate sources of stress intensity factor not included in equation 1. Sources of stress intensity factor not included in equation 1 include, residual stresses in the RPV structural welds (K_{IRS}), stresses produced by pressure on the crack face (K_{IPCF}), and stresses resulting from differential thermal expansion between the stainless steel cladding and the low-alloy steel RPV shell material (K_{ICB}). In the following evaluations, K_{IRS} and K_{ICB} are included, but K_{IPCF} is not included because it has only a minor influence on the results.

Equation (1) can be modified as follows to produce the allowable pressure (P_{CODE}) at a given normalized temperature ($T\text{-}RT_{NDT}$).

$$P_{CODE} = (K_{Ia} - K_{It}) / (2C_P) \quad (2)$$

Where: C_P is the stress intensity factor at the deepest point on the 1/4t flaw produced by a 1 ksi pressure loading in the RPV (ksi$\sqrt{}$in.)

For the calculation of P_{BE} equation (2) was modified as follows to, (a) include all significant sources of applied stress intensity factor, (b) eliminate the safety factor of 2 on pressure loading, and (c) consider a number of definitions of the material fracture toughness (K_{Ix}).

$$P_{BE\theta} = (K_{Ix\theta} - K_{ISC\theta}) / C_{P\theta} \quad (3)$$

and

$$K_{ISC\theta} = K_{It\,\theta} + K_{IRS\theta} + K_{ICB\theta} \quad (4)$$

Where: $P_{BE\theta}$ is the best estimate allowable pressure (ksi).
$K_{Ix\theta}$ is the normalized-temperature-dependant fracture toughness for material definition x (ksi$\sqrt{}$in.).
$K_{ISC\theta}$ is the sum of all strain controlled stress intensity factors (ksi$\sqrt{}$in.).
$C_{P\theta}$ is the stress intensity factor produced at a specified location on the reference flaw in a RPV by internal internal pressure of 1 ksi.
$K_{It\theta}$ is the applied stress intensity factor produced by a through-the-wall temperature gradient (ksi$\sqrt{}$in.).
$K_{IRS\theta}$ is the applied stress intensity factor produced by residual stresses in the RPV structural welds (ksi$\sqrt{}$in.).
$K_{ICB\theta}$ is the applied stress intensity factor produced by clad-base material differential thermal expansion (ksi$\sqrt{}$in.).

The designator θ in the above definitions indicates the critical location on the crack front. Introduction of this designator is necessary because the position of the critical location on the crack front is influenced by the choice of the material fracture toughness definition (x). The critical location for a relatively high material fracture toughness ($K_{Ix\theta}$) is usually at the deepest point on the crack front, but it moves to a location near the clad-base metal interface when $K_{Ix\theta}$ is lower.

2.3 Scope

Fracture toughness of the RPV material was the primary variable in this P-T curve margin assessment. Fracture toughness curves used in the margin assessment included the K_{Ic} and K_{Ia} curves defined in the ASME Code, plus additional curves designated, K_{Icm}, K_{Ic}', and K_{Icsf}. The mean curve (K_{Icm}) through the

EPRI K_{Ic} database was defined in Ref. 7. The data plots of Ref. 7 also show a number of points below the ASME K_{Ic} curve in the normalized temperature (T-RT_{NDT}) range of interest in a P-T curve analysis. The K_{Ic}' curve was obtained by adjusting the ASME K_{Ic} curve downwards by 4.5 ksi$\sqrt{in}$, so that it became a true lower-bound curve for T-RT_{NDT} values down to –200°F. The 1.0" deep 6:1aspect ratio flaw specified for the reference problem has an absolute value of flaw depth, a, that is slightly greater than most of the flaw depths in the shallow-flaw specimens used to generate the shallow-flaw fracture toughness database for RPV materials [8-13]. The reference flaw does, however, have an a/W ratio of 0.11 which is in the mid-range of a/W values for these shallow-flaw specimens. The judgement is then that toughness values developed in the shallow-flaw test programs should envelope the minimum toughness value expected for the reference flaw. The lower-bound to the shallow-flaw fracture toughness data (K_{Jcsf}) is 7.5 ksi$\sqrt{in}$ above the ASME K_{Ic} curve at all T-RT_{NDT} values. The K_{Icsf} curve was generated by adjusting the ASME K_{Ic} curve upward by 7.5 ksi$\sqrt{in}$ so that it became a lower-bound curve for shallow flaw fracture toughness data.

3. Materials Properties

3.1 Fracture toughness bounding curves

The mean fracture toughness curve used in these studies was taken from the evaluation of the EPRI K_{Ic} database as described by Nanstad, et al., in Ref. 7. After a thorough check of the toughness values reported in the original EPRI database, some corrections and deletions of invalid data were made. Using the corrected database, a mean curve was developed using a non-linear regression analysis and an equation of the form of the ASME Section XI K_{Ic} curve. The database and mean curve, with constants as reported in Ref. 7, are shown in Fig. 2.

The ASME Section XI K_{Ic} and the K_{Ic}' curves are also shown in Fig. 2. The K_{Ic}' curve was constructed by shifting the Section XI K_{Ic} curve downward to pass through the lowest data point of the EPRI data set. Only data above T-RT_{NDT} = -200°F were considered since lower normalized temperatures are not relevant for P-T curve evaluations. Using the philosophy of a "below all points" curve, the controlling data point was found to be for HSST Plate 01 material tested at T-RT_{NDT} = -170°F, K_{Ic} = 29.4 ksi$\sqrt{in}$. This point is 4.5 ksi$\sqrt{in}$ below the ASME Section XI K_{Ic} curve at that normalized temperature. The equation for the K_{Ic}' curve is then,

$$K_{Ic}' = 28.7 + 20.734 \exp[0.02(T - RT_{NDT})] \quad (5)$$

Note that the curves discussed above represent the toughness for deep-flaw specimens. For this study, it was desired to develop a shallow-flaw lower-bound fracture toughness curve comparable to the ASME Section XI K_{Ic} curve. The curve developed could then be used for the P-T curve margin evaluations. Test programs to investigate shallow-flaw fracture toughness in RPV materials have been performed by ORNL and the Naval Surface Warfare Center (NSWC) [8-13]. The specimens used were beam-type structures with either 2-D or 3-D through-surface flaws. For the ORNL testing, specimens were subjected to uniaxial or biaxial loading. In general, it was concluded that shallow flaws have greater scatter and higher mean fracture toughness than deep flaws, but that there appeared to be little difference in the lower-bounds for either data set [14]. For the purposes of this study, the shallow and deep-flaw data sets were re-evaluated to quantify, as best possible, the comparative effects on fracture toughness of shallow

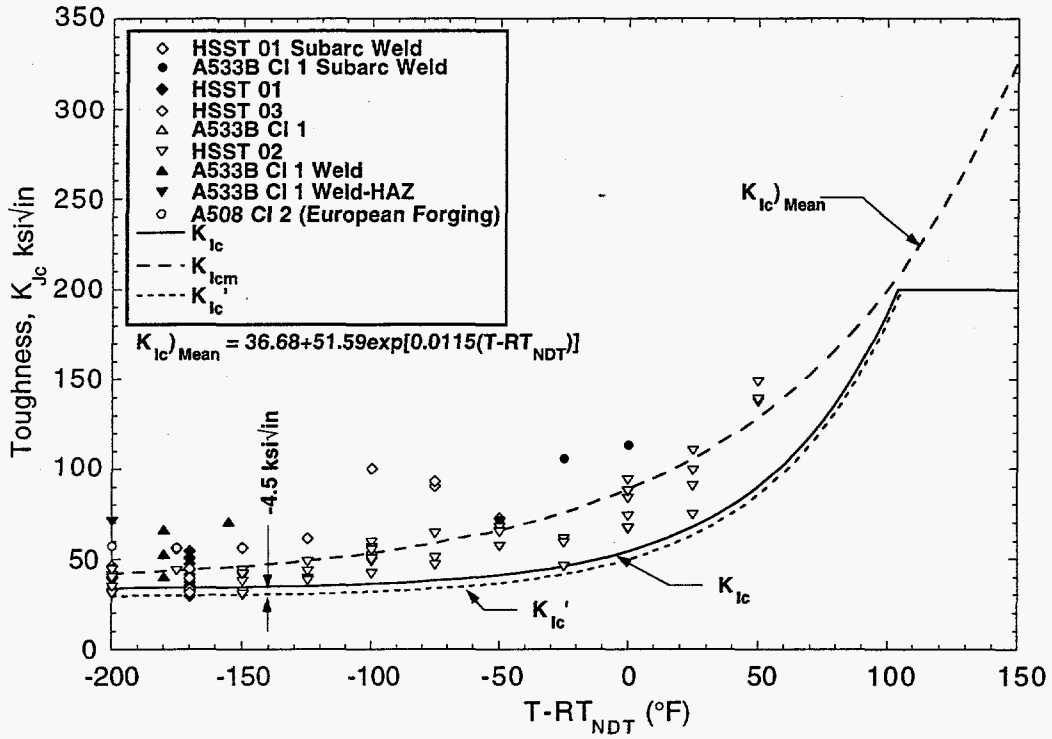

Fig. 2 EPRI database showing position of K_{Ic}, K_{Ic}', and K_{Icm} fracture toughness curves.

versus deep flaws. The value of the test programs performed by ORNL and NSWC is that comparative shallow and deep-flaw specimens were tested using the same materials and test conditions. The materials were all A 533 B steel with heat treatment applied to some heats to achieve elevated yield strength. Thus, direct inferences may be drawn as to shallow-flaw effects. To evaluate shallow-flaw effects, the data were restricted to specimens with 2-D surface flaws to have similarity in specimen geometry. The 2-D flaw data are shown in Fig. 3. Examination of this figure reveals immediately the conclusion that shallow-flaws exhibit greater scatter in fracture toughness, than do deep flaws. To quantify the difference in the mean toughness between shallow and deep-flaws, these data were analyzed using standard non-linear regression methods. Equations of various forms were tried, but the best correlation was obtained using a simple exponential equation of the form,

$$K_{Jc} = a_1 \exp[a_2(T - RT_{NDT} + a_3)]. \tag{6}$$

An equation of this form penalizes the mean toughness values at low temperatures since, in the limit, it approaches zero as an asymptote. In this sense, its use is conservative. It does, however, have the advantage that no artificially imposed lower-bound is applied. Regression analyses yielded the constants as shown in the Table 1 below. The mean curves for both shallow and deep-flaws are shown in Fig. 3. The lower-bound for the shallow-flaw curve was constructed by inspection, rather than statistical treatment, i.e., utilization of some multiple of the standard deviation of the fit. The lower-bound curve was established as a fractional multiplier of the mean curve, with the multiplier being selected such that the resulting curve bounded all shallow-flaw data. The resulting lower-bound is shown in Fig. 3. It was

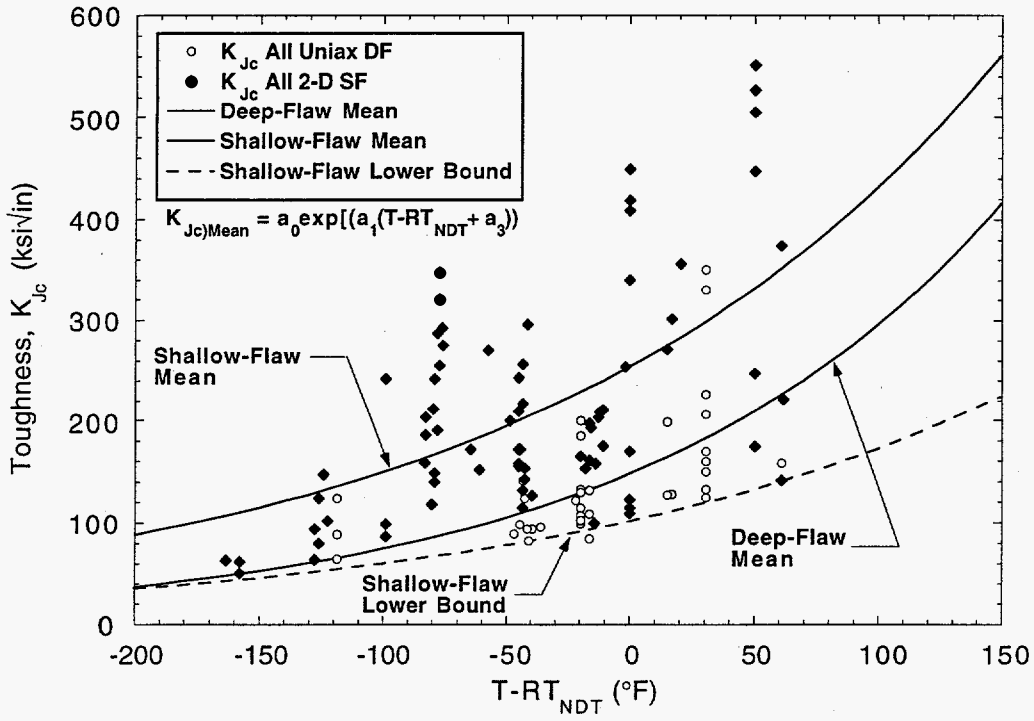

Fig. 3 Comparison of shallow- and deep-flaw data sets with mean curves showing elevation of shallow-flaw fracture toughness.

observed from the data shown in Fig. 3 that, where sufficient numbers of shallow and deep-flaw specimens were tested under the same conditions, the mean value and lower-bound of the shallow-flaw data are greater than the mean and lower-bound of the deep-flaw data. (See for example the tests performed over the range $-50°F \leq T\text{-}RT_{NDT} \leq 0°F$.) For P-T limit evaluations contained in this paper, the lowest normalized temperature ($T\text{-}RT_{NDT}$) is greater than –170°F. At –170°F, the shallow-flaw lower-bound curve shown in Fig. 4 is 7.5 ksi√in above the ASME Section XI curve. Since the Section XI K_{Ic} curve is programmed into the analysis procedures, for ease of application the K_{Jcsf} lower- bound curve was established by raising the K_{Ic} curve by 7.5 ksi√in as is shown in Fig. 4.

Also, included in Fig. 4 is a set of 3-D shallow-flaw clad cruciform beam test results for RPV weld material. These specimens were tested under uniaxial (0:1) and biaxial (1:1) loading from which it was determined that the constraint associated with biaxial loading reduces fracture toughness compared to uniaxial loading, as shown in Fig. 5. The K_{Jcsf} curve in Fig. 4 bounds all the clad cruciform results, with those lying closest to the curve being biaxially loaded tests. It is then concluded that the K_{Jcsf} lower-bound curve shown in Fig. 4 provides a rational and conservative lower-bound to RPV material shallow-flaw toughness data.

As was previously discussed, the K_{Ia} curve was specified for P-T curve analysis because of concerns about the effect of local brittle zones on static fracture toughness [7]. Recent test results indicate that local brittle zones have no significant effect on static fracture toughness [4]. It is then concluded that current activities within the ASME Code to permit use of the K_{Ic} curve instead of the K_{IR} curve have a sound technical basis.

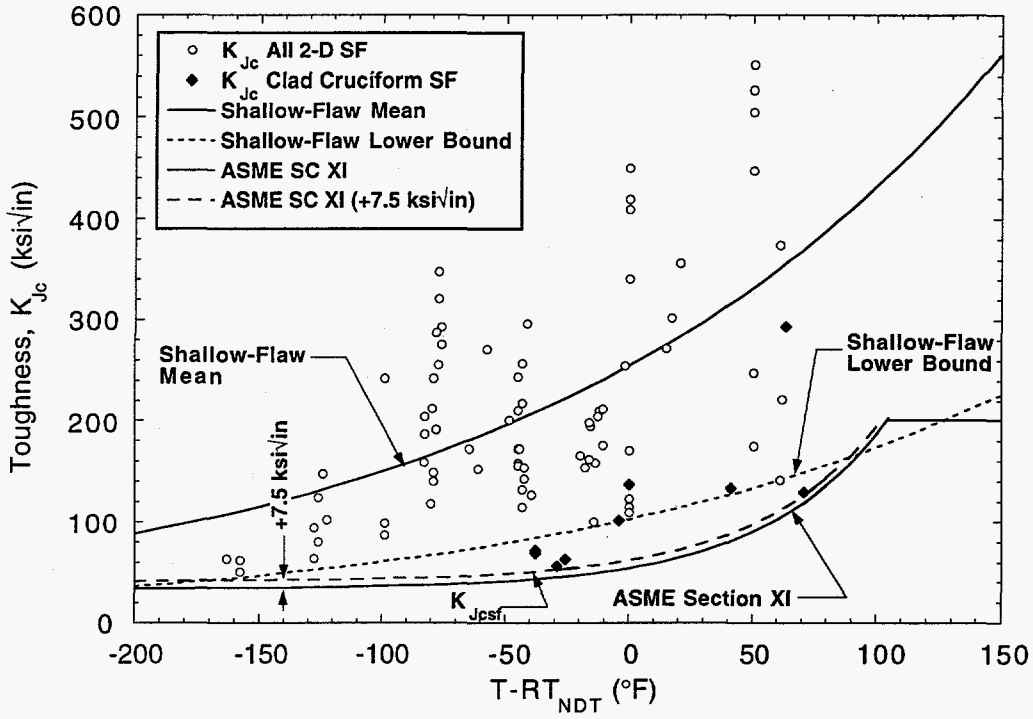

Fig. 4 Shallow-flaw fracture toughness data set with recommended lower-bound, K_{Jcsf}.

Table 1

Constants for the Shallow-Flaw and Deep-Flaw Mean Curve Equations

Flaw Type	a_1	a_2	a_3
2-D Shallow	51.211	0.0069	153.79
2-D Deep	80.465	0.0053	216.96

3.2 Fracture Behavior of Clad Material

In order to evaluate the behavior of subclad flaws and their influence on RPV integrity, some definition of the clad layer failure criteria was needed. For this purpose, data generated using a special Jo-Block specimen was used. The Jo-Block specimen was first conceived for the purpose of evaluating the fracture properties of cladding over a subclad flaw. The specimen consists of two machined steel blocks with the ends butted together to form a "crack." The name Jo-Block was derived from Johansson blocks, which are precision-machined gage blocks used for calibrating instruments, etc. Two machined blocks are butted together, and cladding is deposited on opposite faces of this assembly across the interface between the two blocks. Subclad flaw tips are then generated at the intersection of the block interfaces and the

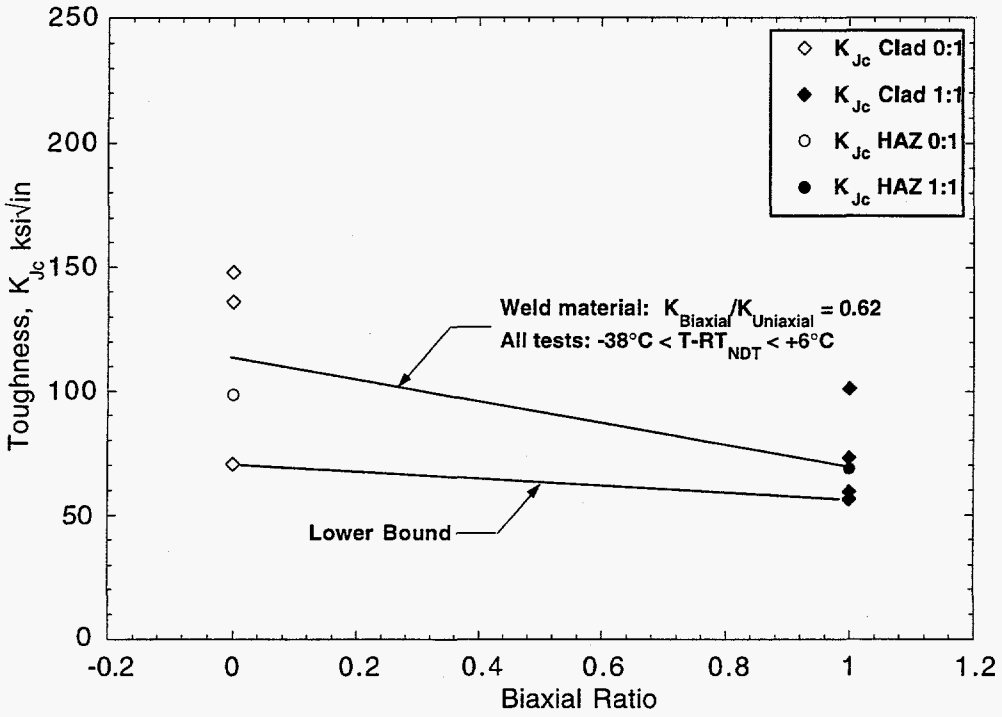

Fig. 5 Biaxial loading causes a reduction in the mean and lower-bound fracture toughness in RPV weld material.

overlying cladding. The quality of the butted-machined surfaces, the care used in fit-up and the restraint against distortion during cladding determine the final width of the crack. In practice, essentially zero-width cracks were obtained with relatively "sharp" flaw tips, i.e., tip radii in the range of 0.0008–0.003." Shrinkage of the cladding during cooling usually caused additional subsurface crack extension (microcracking) such that the flaw tip had characteristics of a "true" crack. The final crack configuration resembles a cross-section of the clad/base metal interface region of a two-dimensional subclad flaw in a vessel wall. Since the cladding is applied in the same manner that vessel cladding is applied, the cladding retains many of the characteristics that cladding on a vessel wall would have. The details of fabrication of these specimens are contained in Ref. 15. An isometric drawing of the Jo-Block specimen is shown in Fig. 6.

The effective yield stress and the rupture strain of the cladding and the crack opening displacements (COD) beneath the cladding were determined. The amount of clad surface stretching directly over the flaw tip was measured using conventional foil-type strain gages, and clip gages on the sides of the specimen were used to measure COD beneath the clad layer and at the specimen midplane.

The specimens were tested at both room temperature, and at –200°F. A typical plot of front-surface clip-gage readings versus load for a specimen tested at –200°F is shown in Fig. 7. The maximum load for this test was 31.7 kips giving an engineering ultimate strength of 83.5 ksi. Plastic instability in the clad layer occurred for crack-tip opening displacements in the range of approximately 0.010- to 0.020." Failure of the cladding occurred at a COD greater than 0.032." Specimen failure was characterized by failure in only one ligament of cladding. When yielding occurred in one clad surface as shown in Fig. 7, there was little further increase in load. The yielded surface became the "weak link" and continued to stretch up to

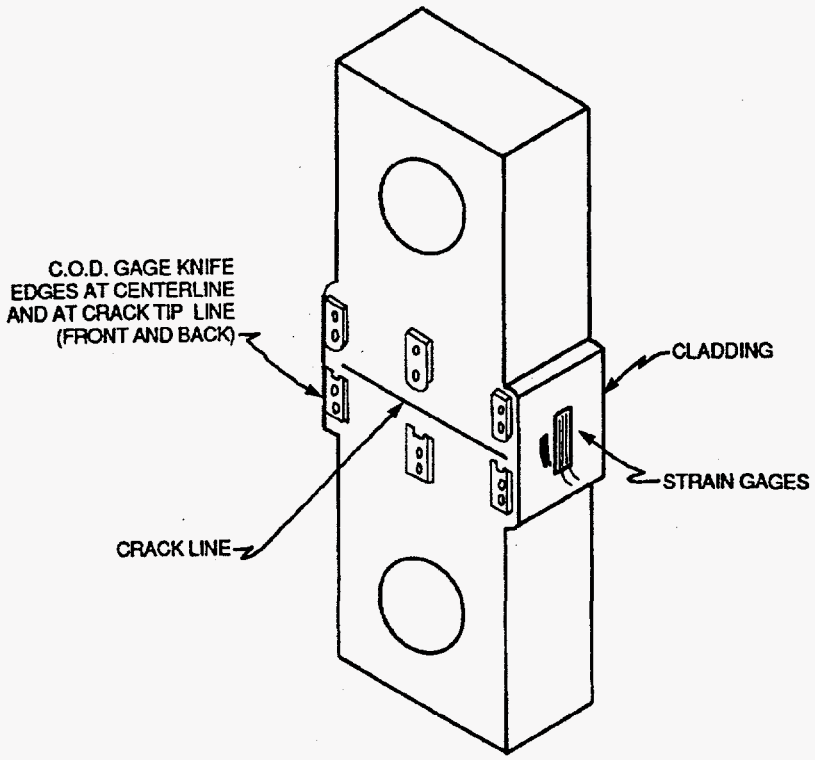

Fig. 6 Isometric drawing of Jo-Block specimen used to measure properties of clad layer over subclad flaw.

failure of the cladding. Since there was little additional load increase, axial deformation and COD of the opposite surface essentially stopped. Figure 8 is an enlarged view of the initial part of this loading curve, which shows three distinct regions of behavior. The first of these, which extends up to a load of approximately 6 kips is the elastic response of the entire specimen (base metal and cladding), and is due to the pre-load caused by the cladding residual thermal stress. This is indicated as the "Elastic Bar" line in Fig. 8. The second region is the near linear elastic behavior of the cladding acting alone. Nonlinear response of the cladding initiates at approximately 18 kips. The last region is the fully non-linear plastic behavior of the cladding. For the cladding, taking the deviation from non-linear behavior as the "yield" point, an effective clad yield stress for this configuration of 47 ksi would is obtained.

The failure of these specimens was characteristically by ductile tearing of the cladding and plastic instability even at –200°F. There was no evidence of cleavage-type fracture. The deformation results above are used in the assessment of clad instability given in Section 4.

3.3 Residual Stresses in Cladding and Weld

Residual stresses were measured in the longitudinal weld and in the clad layer of an RPV shell segment. Procedures utilized and the results obtained are briefly described below.

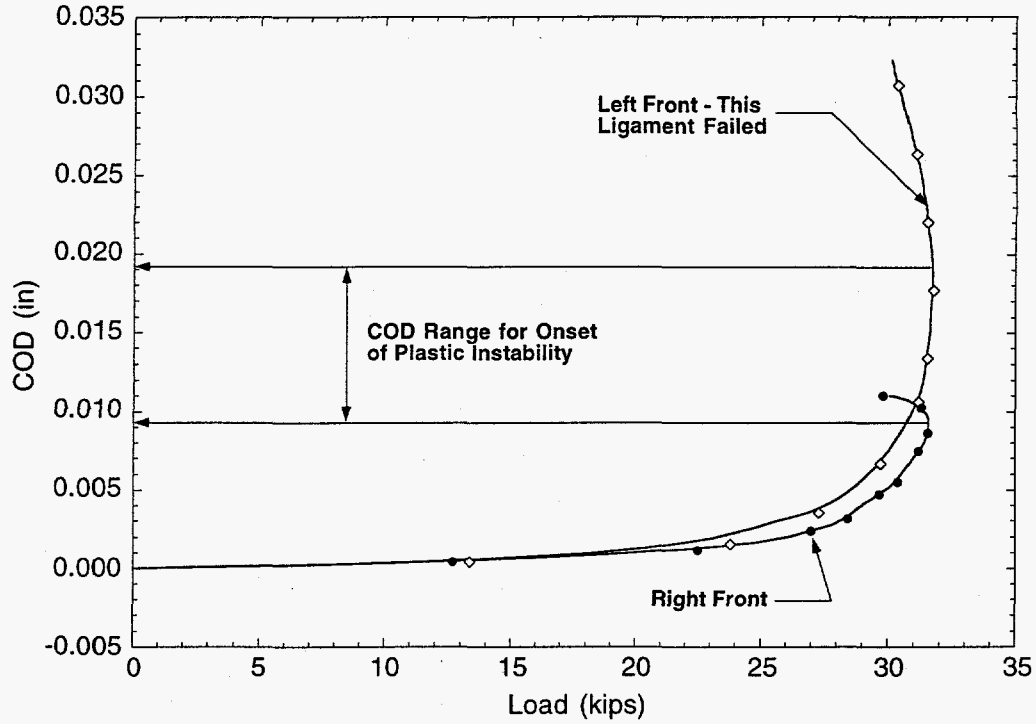

Fig. 7 Load-COD behavior of typical Jo-Block specimen showing highly ductile deformation characteristics of clad layer.

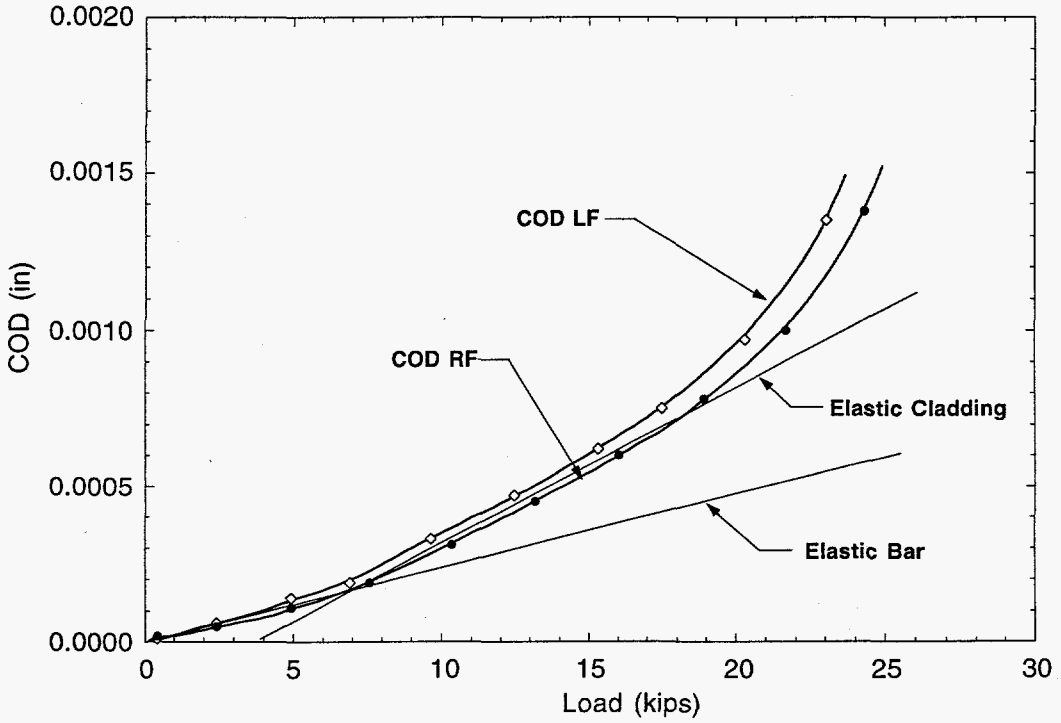

Fig. 8 Initial elastic region of Load-COD behavior for Jo-Block specimen shown in Fig. 8.

3.3.1 Longitudinal weld residual stress

The residual stresses in a RPV structural weld stem from (a) the clad-shell differential thermal expansion (DTE) and (b) the residual stresses, generated by the structural welding process, that are not completely relaxed by the post-weld heat-treatment [11]. Data required for calculation of these residual stresses were obtained by cutting a radial slot in the longitudinal weld in a shell segment from a RPV, and measuring the deformation of the slot width after cutting. The measured slot openings are assumed to be the sums of the openings due to the clad-base material differential thermal expansion (DTE) and the weld residual stresses. To evaluate the residual stresses in an RPV structural weld, a combined experimental and analytical process was used. Slot opening measurements were made during the machining of full-thickness clad beam specimens with 2-D flaws. The blanks measured 54" long (circumferential direction), 9" wide (longitudinal direction), and 9" thick (radial direction). The blanks were cut so as to have a segment of a longitudinal seam weld from the original RPV at the mid-length of the blank. Using the wire-EDM process, a slot was cut along the weld centerline in a radial direction from the inside (clad) surface of the blank. Measurements were made on three specimens having final slot depths of 0.045," 0.90," or 4.50," respectively. After machining, the widths of the slots were measured along each radial face of the blanks. The results for the specimen with a 4.50" deep flaw are shown in Fig. 9. Finite element analyses were used to develop a through-thickness stress distribution that gave a deformation profile matching the measured values. This distribution is shown in Fig. 10, where the contribution from clad and base DTE has been removed.

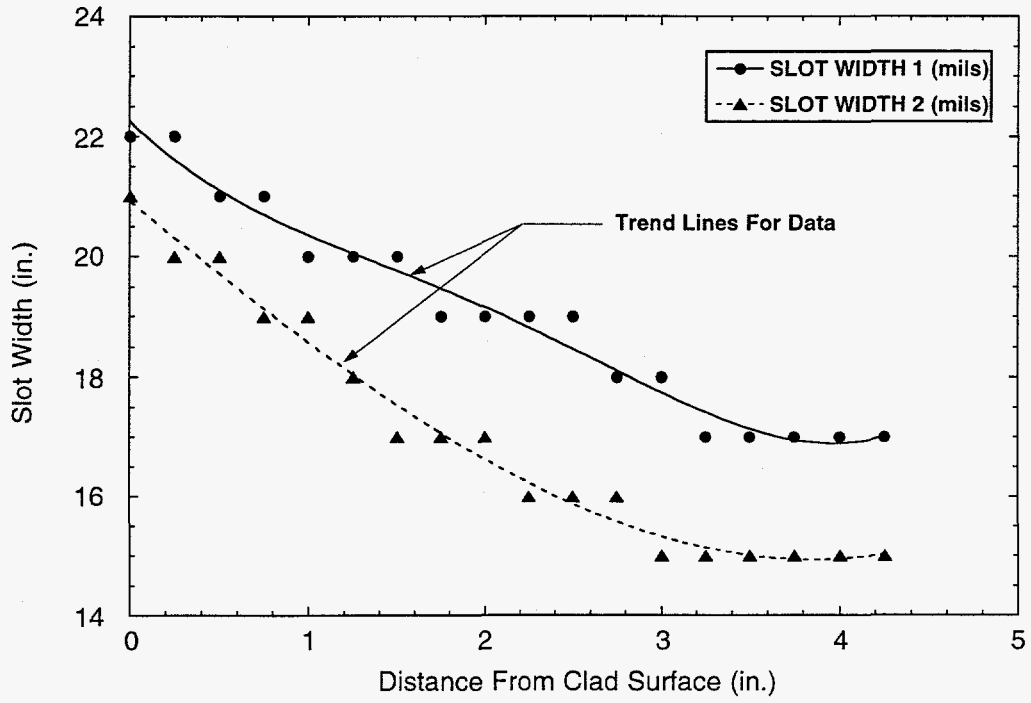

Fig. 9 Slot-opening measurements made for RPV weld specimen with 4.5" deep flaw.

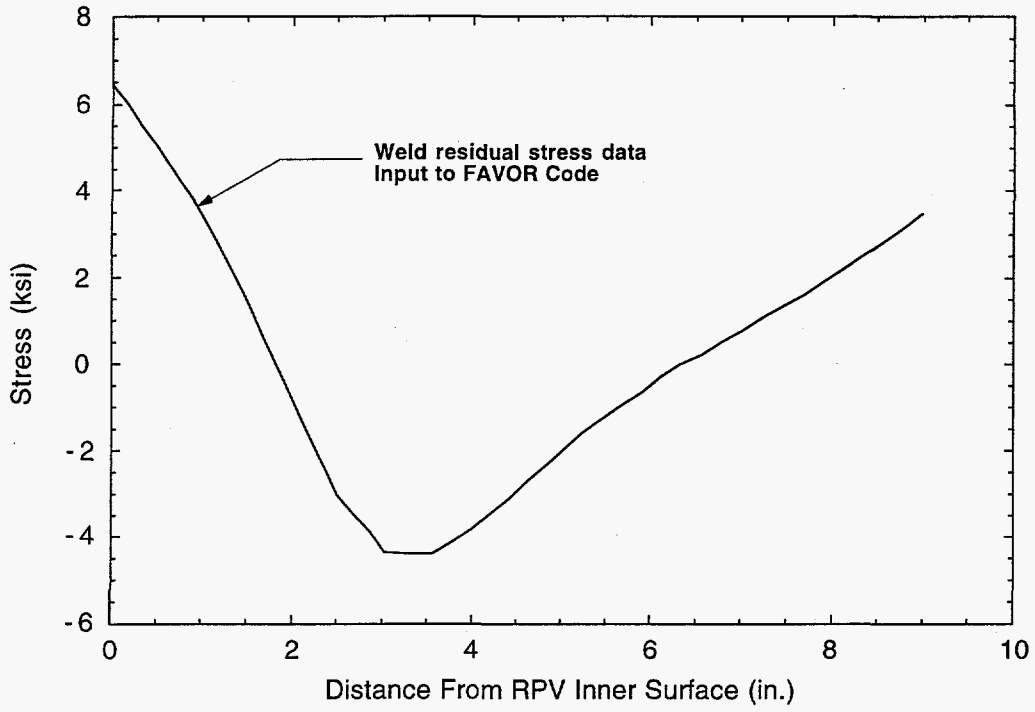

Fig. 10 Final weld residual stress through-thickness distribution developed for use in RPV integrity analyses.

3.3.2 Cladding residual stress

The procedure used for a determination of the residual stresses in the clad material was to separate the clad layer from the underlying plate material, measure the change in geometry during this procedure, and calculate the clad stresses relieved. As a test article, a block of the clad-over-plate shell material measuring 10" square and full-RPV-wall thickness was used. Two smaller full-thickness blocks were then saw-cut from this block. Each of these smaller blocks was machined to a parallelepiped 4" x 1" x 9 1/4" thick (shell thickness). One block was taken with the clad layer length (4" dimension) in the circumferential direction of the shell (parallel to the cladding deposition direction) and the other in the longitudinal direction (transverse to the cladding deposition direction). The sequence of operations and the orientation of the clad strips relative to each other are shown in Fig. 11. As part of the machining process, inspection points (fiducial marks) were applied at points on the original and machined-end surfaces of the clad layer. These points were drilled to a depth not exceeding 0.010" using a conical point drill. This procedure assured an inspection point with uniform dimensions for repeatability of the subsequent measurements.

Precision dimensional inspections were performed to measure the x, y, and z coordinates of each of these fiducial marks with the blocks in the parallelepiped geometry. A set of coordinate axes is shown in Fig. 11 for reference. After the initial dimensional measurements, the clad layer was machined away from the plate material until the clad/base metal fusion zone was completely revealed. To estimate the mid-thickness of the fusion zone, visual inspection was used to judge when approximate equal amounts of

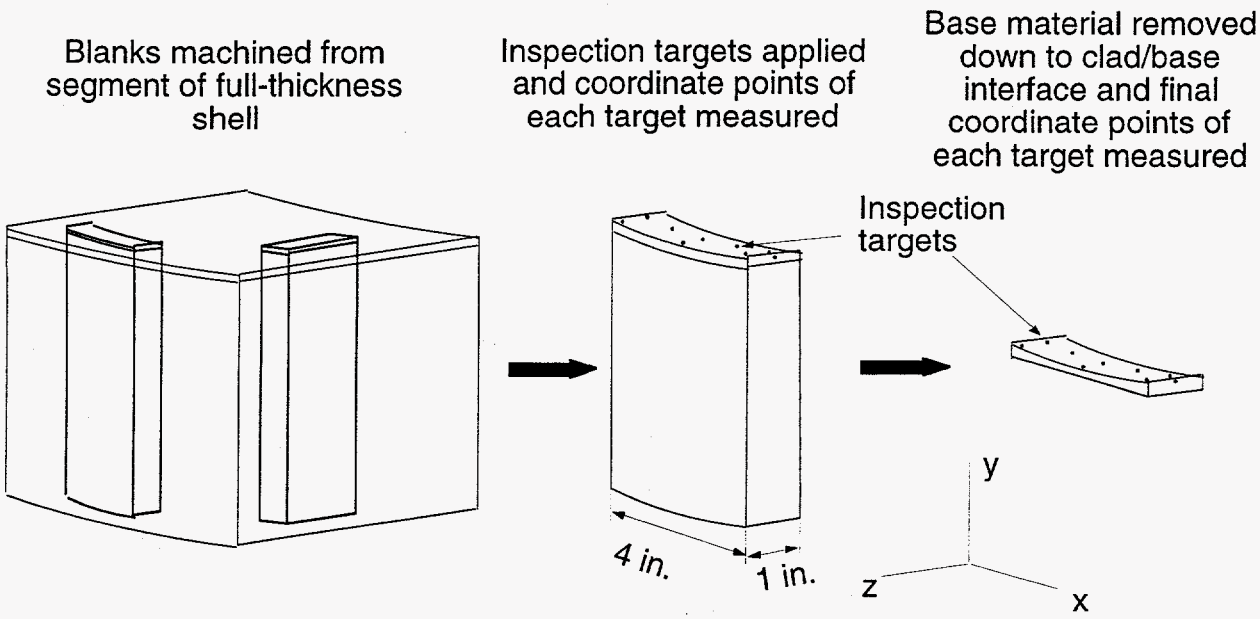

Fig. 11 Schematic of operations used to obtain strain measurements from relaxation of residual stresses in clad layer.

plate and clad materials were exposed on the machined surface. The clad layer parts were re-inspected to measure the distorted shape as compared to the original shape. The change in shape of the parts was then determined by subtracting the initial coordinates of each inspection point from the final (deformed) coordinates. Using the deformed coordinates for each fiducial mark, maximum and average values (for the sets of measurements) of circumferential and longitudinal strain were calculated and are shown in Table 2.

Table 2

Strains Measured when Cladding was Released from

the Base Material of a RPV Shell Segment

	Strain ε_x (in/in)	Strain ε_y (in/in)
Maximum	-0.00086	-0.00041
Average	-0.00070	-0.00033

These strains were used as boundary conditions in finite-element analyses to determine the maximum and average values of clad residual stress components. It was first necessary, however, to determine the appropriate value of elastic modulus for the clad strip since, as was described above, the final clad strip contained both clad and fusion zone material. From tensile tests of both clad and fusion zone material at –30°F, the effective modulus of the clad strip was determined to be,

$E_3 = 24.85 \times 10^6$ psi.

The modulus, E_3, is for the composite clad strip at -30°F, while the residual stress measurements were performed at room temperature. To calculate the elastic modulus at room temperature, a third-order polynomial in temperature was fitted to the ASME data for 18 Cr - 8 Ni steel; see Table TM-1, p. 664, ASME Boiler and Pressure Vessel Code, Section II, Part D, 1992. The equation was then normalized to the value of E_3 at –30°F yielding a temperature dependent modulus for the clad strip of,

$$E = a_0 + a_1 T + a_2 T^2 + a_3 T^3, \tag{7}$$

where T = temperature in °F,
and $a_0 = 24.71$
$a_1 = -0.005257$
$a_2 = -4.6257 \times 10^{-7}$
$a_3 = -3.5109 \times 10^{-11}$.

The value of modulus for the equivalent clad layer at room temperature is then,

$E_{RT} = 24.30 \times 10^6$ psi.

Using this value of modulus and a Poisson's ratio of 0.3, the resulting residual stresses from the finite-element analyses for the two cases considered (maximum and average strains) are shown below.

Strain Combination	Circumferential Stress (ksi)	Longitudinal Stress (ksi)
Maximum	26.2	17.8
Average	21.3	14.4

It is appropriate to also consider the contribution of the "curling" deformation of the clad strip to the overall residual stress-state. Considering the strip as a thin, cantilever beam with applied displacement of the free end, the residual bending stress in the clad strip was calculated to be in the range of 1 ksi. The bending stresses in the clad layer were then considered to be an insignificant part of the of the total residual stress state and would have minimal impact on the determination of a stress-free temperature.

3.3.3 Stress-free temperature

The residual stresses determined for the clad layer were used to calculate the stress-free temperature for the vessel. Since the circumferential and longitudinal stresses will not necessarily go to zero simultaneously, only the circumferential (larger) stress component was used to determine the stress-free temperature. Also, since the margin assessments performed and described below were to represent "best

estimate" results, the average value of circumferential stress was used. Using the FAVOR Code, the stress-free temperature was calculated to be,

$$T_{stress\text{-}free} = 468°F.$$

4. Clad Stability Evaluation

The evaluation of cladding integrity under P-T curve loading conditions was done to determine if the cladding above a subclad flaw would remain structurally intact throughout the operating life of a RPV. Pressures associated with potential breaching of the cladding are designated (P_c) in order to distinguish them from the best estimate allowable pressures (P_{BE}) for the RPV shell. The failure modes of primary concern relative to the evaluation of P_c for irradiated cladding above a subclad flaw are (a) tensile instability at room temperature, and (b) ductile tearing at the RPV operating temperature. The process of cladding over a subclad crack has been shown to produce sharp micro-cracks in the cladding above the flaw [15]. These micro-cracks could be further extended by ductile tearing of the irradiated cladding.

ORNL has performed an elastic-plastic finite element analysis of a subclad flaw in a RPV using the finite element analysis model shown in Figs. 12 (a) and (b). COD results from that analysis are shown plotted as a function of pressure loading in Fig. 12(c). The response of cladding above a flaw to tensile loading was described in Section 3. COD results obtained from the tests are shown in Figs 7 and 8. Fig. 8 shows that the onset of tensile instability occurred when the COD reached approximately 20 mils. This COD value is substantially higher than the value (2.2 mils) obtained in Fig. 12 (c) at the operating pressure (2.2 ksi). Tensile instability of the cladding above a subclad flaw would not, therefore, be expected to occur under a single application of either operating loads or hydrotest loads.

Since the cladding process can introduce a sharp crack into the cladding immediately above a subclad flaw [15], the potential for further propagation of that crack by ductile tearing must be evaluated. Ductile tearing initiation data (K_{Jc}) for 3-wire stainless steel cladding, irradiated to a fluence of 2.41×10^{19} n/cm^2, are shown as a function of temperature in Fig. 13 [16]. The geometry of the subclad flaw in the elastic-plastic finite-element analysis model of Figs. 12 (a) and (b) was extended .025" into the cladding to permit the calculation of K_J values applied to the cladding. Results from the analysis of K_{JSC} values for all strain-controlled loading are shown superimposed on the tearing toughness curve of Fig. 13. The temperature-dependent difference $K_{JPC} = K_{Jc} - K_{JSC}$ is the ductile tearing toughness available for accommodation of pressure-induced stress intensity factors. A curve of K_{JPC} is also included in Fig.13. The minimum value of K_{JPC} was obtained as 48 ksi$\sqrt{in}$. at a temperature of approximately 480°F. Analysis results show the stress intensity factor (C_P) produced by a 1 ksi pressure loading in the RPV to be 30.3 ksi$\sqrt{in}$ for the stainless-steel portion of the sub-clad flaw. The limiting pressure for prevention of the onset of ductile tearing in the cladding above the subclad flaw is, therefore, $K_{JPC}/C_P = 48/30.3 = 1.6$ ksi. Since the operating pressure for the RPV at a temperature of 550°F would be of the order of 2.2 ksi, tearing of cladding above the subclad flaw would be predicted.

The RPV manufacturing process would tend to produce subclad rather than surface-breaking flaws. Results from the above evaluation, however, indicate that the microcracks introduced by the cladding process and ductile tearing could result in breaching of the cladding, thereby converting the subclad flaw to a surface-breaking flaw. This finding prevents the use of a sub-clad flaw for P-T curve margin assessments. Limited evidence exists showing that cladding over a pre-existing sharp crack can produce a reduction in fracture toughness of the crack-tip material, by the action of locally intensified strain aging (LISA) embrittlement. The LISA embrittlement mechanism could be of concern if subclad cracks

convert to surface cracks by the process described above. At this time, however, the body of data available on cladding-induced LISA embrittlement is not sufficient for an evaluation of its potential impact on P-T curve margins.

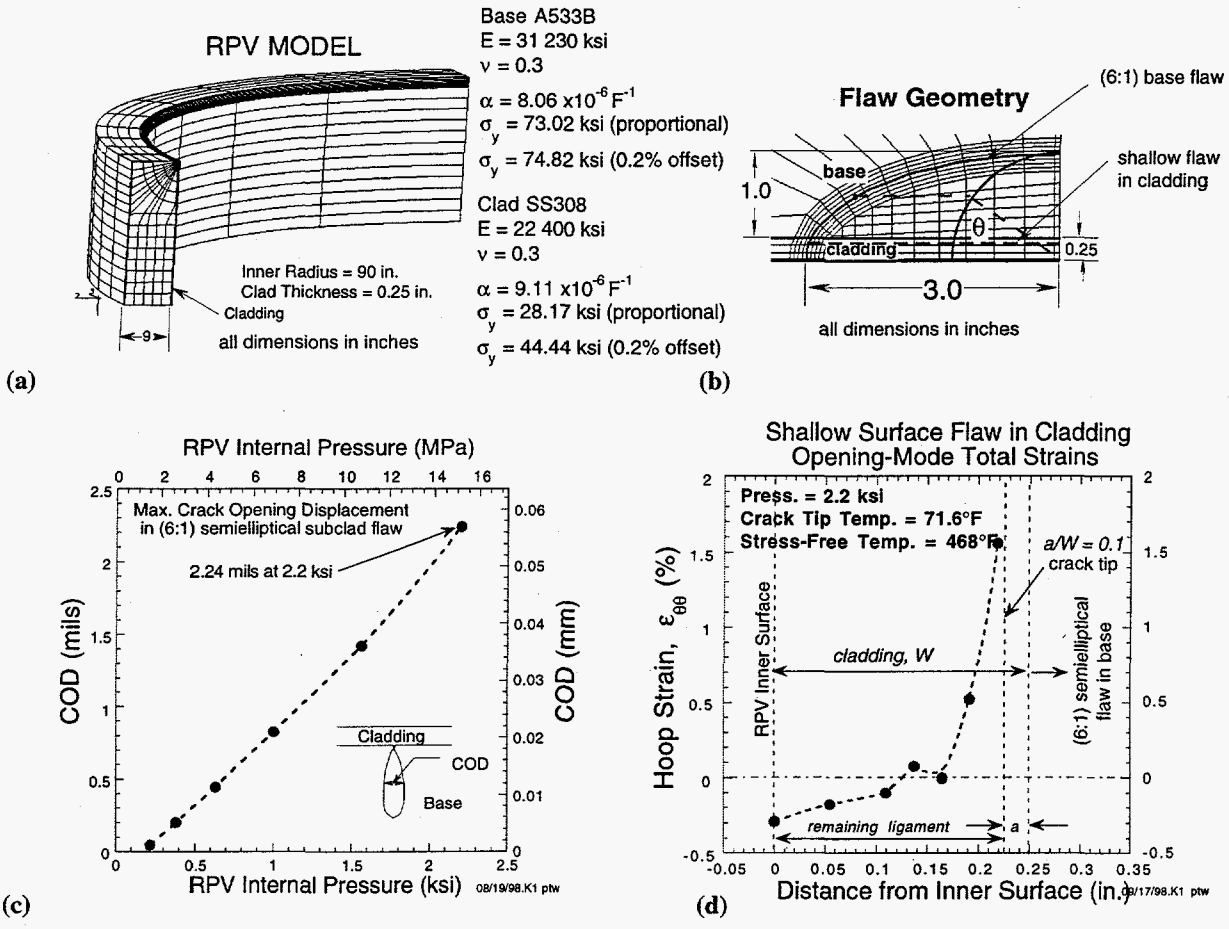

Fig. 12 Finite-element analysis of a semielliptical subclad flaw: (a) RPV model, (b) subclad flaw geometry, (c) crack-opening displacement, and (d) hoop strain profile across cladding with shallow flaw (a/W=0.1) opening to larger flaw in base.

5. Margin Assessments

A reference problem was defined under NRC guidance such that various organizations could perform deterministic fracture analyses to benchmark solutions. The objective for this study was to compare the fracture margin derived from a best-estimate-analysis that includes all of the loads, to the fracture margins derived from the current ASME code and the proposed change to the current code, both of which include only the load due to pressure and the through-wall thermal gradient. The description of the benchmark reference problem is as follows:

The RPV specified for the sample problem has an inside radius of 90," a wall thickness of 9," and a clad thickness of 0.25." Thermal-elastic properties are specified for the sample problem as given in Table 4. The temperature-time history of the cool-down transient is as shown in Fig. 14. The neutron fluence at the inner surface of the RPV was specified as 1.01×10^{19} n/cm^2; the copper and nickel weight percent concentrations were set at 0.30 and 0.86, respectively; and an initial unirradiated value of RT_{NDT} defined

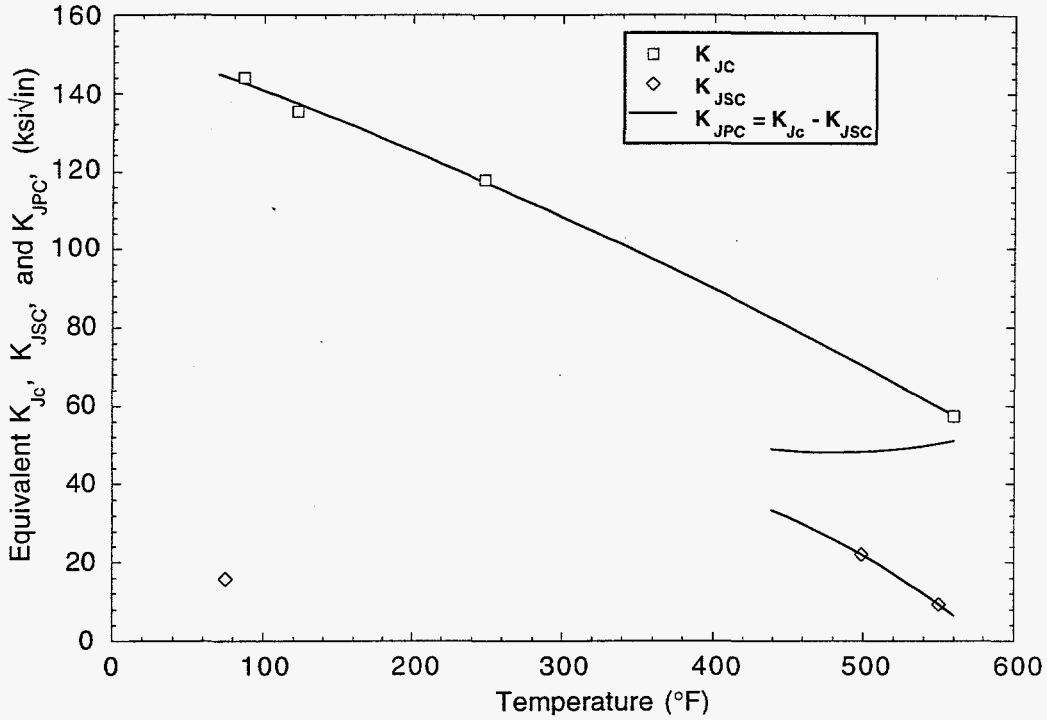

Fig. 13 Stress intensity factor available to resist tearing in the cladding.

Table 4
RPV thermal-elastic material properties

	clad	base
Thermal conductivity (BTU/hr-ft-°F)	10.0	24.0
Specific heat (BTU/lb-°F)	0.12	0.12
Modulus of elasticity (ksi)	22800	28000
Thermal expansion coefficient (°F^{-1})	9.45×10^{-6}	7.77×10^{-6}
Density (lb/ft^3)	489	489

was defined as 0°F. This combination of parameters produced a value of RT_{NDT} at the inner surface of the vessel of 236°F. The convective heat transfer coefficient at the inside surface of the RPV was set at 1000 BTU/ hr-ft^2-°F.

The postulated defect is an axially oriented semielliptical flaw with an aspect ratio (total length/depth) of 6:1 with a depth of 1" (t/9). The postulated flaw is assumed to be a through-clad inner-surface defect. Figure 15 illustrates the postulated defect. The elliptical parametric angle (θ) is measured around a semicircle the origin of which is at the center of the flaw on the inner surface of the vessel. The semicircle has a radius equal to the flaw depth. The angular crack front location is measured from the inner surface of the vessel (θ=0°), to the deepest point (θ=90°). For this postulated crack, the clad-base

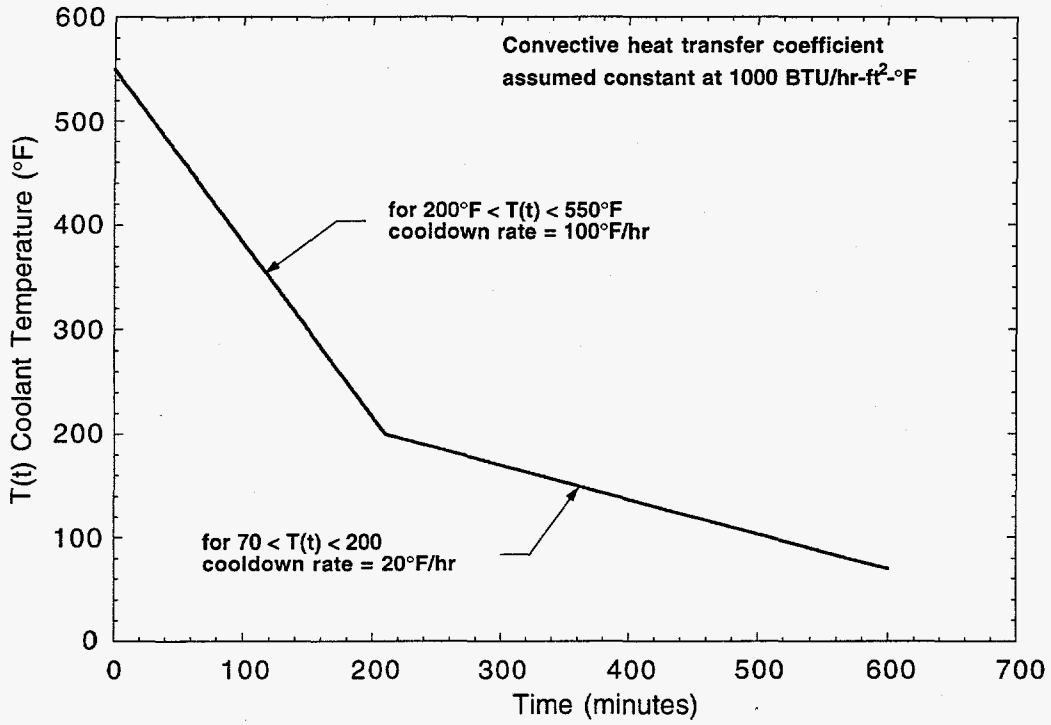

Fig. 14 Benchmark problem cool-down transient.

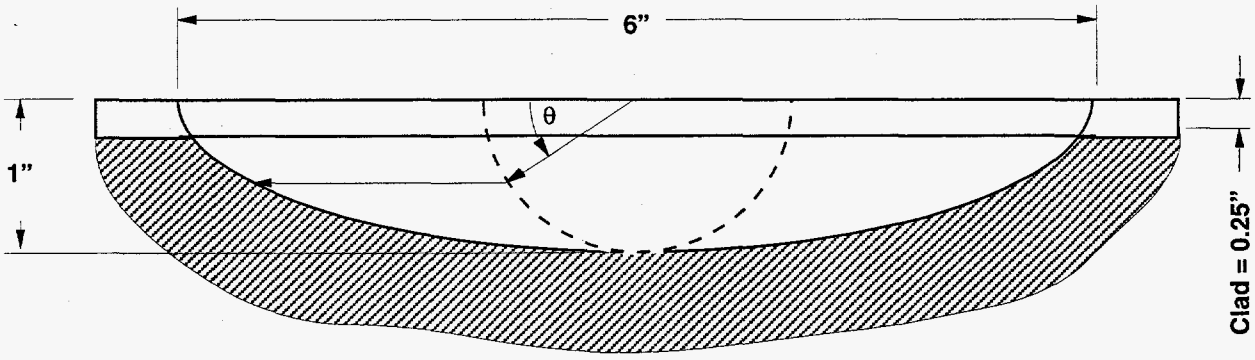

Fig. 15 Schematic showing relationship between circular and elliptic angles used to define points along crack front. The deepest point is at $\theta = 90°$.

interface is at a parametric angular location of approximately 15° degrees. The best-estimate analysis includes searching for the point of initiation around the crack front from the clad-base interface to the deepest point of the flaw, since there are gradients in both the stress intensity factor and cleavage fracture initiation toughness around the crack front.

All deterministic fracture analysis results reported below were generated with the FAVOR computer code [17]. The FAVOR code uses the finite element method to perform thermal and stress analyses, utilizes stress intensity factor influence coefficients [18-20], and superposition to calculate K_I values. FAVOR has been validated to generate solutions that are within approximately 1-2% of those obtained by direct ABAQUS [21] 3-D finite element solutions [22]. ABAQUS is a nuclear quality assurance certified (NQA-1) general purpose multidimensional finite element code that has fracture mechanics capabilities.

Figure 16 shows the superposition of the time histories of stress intensity factor at the clad-base interface (at 15° degrees) due to weld residual stress, clad-base differential thermal expansion, and the through-wall thermal gradient produced by the benchmark transient in Fig. 14. The through-wall weld residual stress was derived in the HSST program from a combination of experimental measurements taken from a RPV shell segment made available from a cancelled pressurized-water reactor plant and finite element thermal and stress analyses [23]. A stress-free temperature of 468°F, derived using the room temperature clad stresses developed in Section 3.3.2, was used in the derivation of the load due to clad-base differential thermal expansion. Figure 16 also shows the time history of the total stress intensity factor at the deepest point (90°) of the flaw. After a time of 200 minutes, the total stress intensity factor is higher at the clad-base interface than at the deepest point of the flaw.

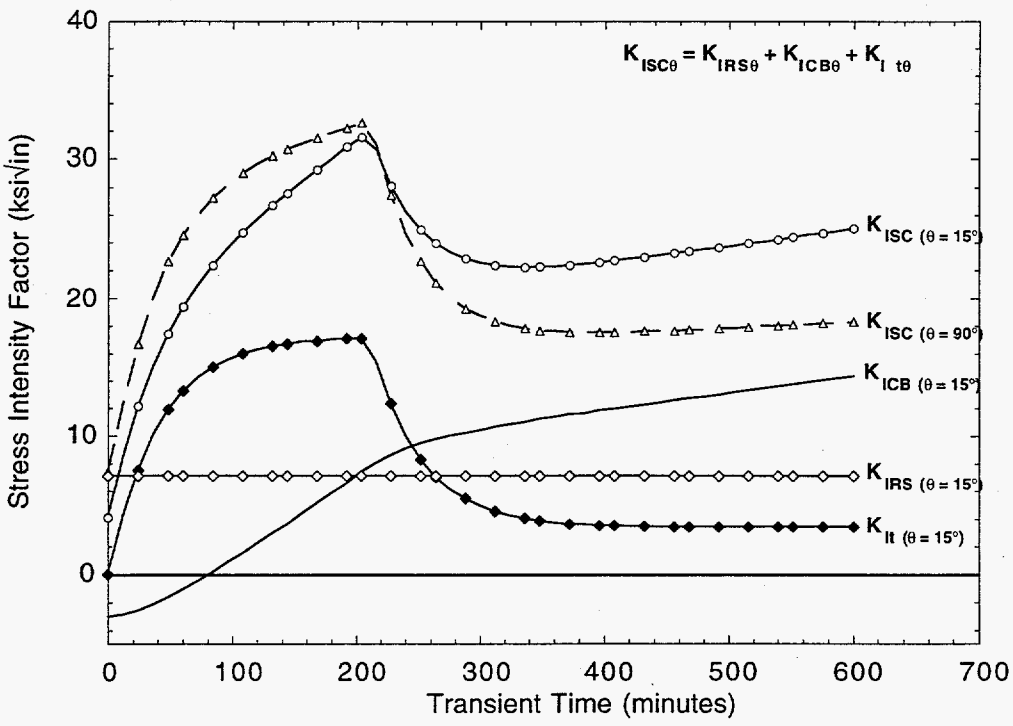

Fig. 16 Superposition of strain-controlled K_I at clad-base interface ($\theta = 15°$) and total strain-controlled K_I at deepest point of flaw ($\theta = 90°$).

Figure 17 illustrates P-T curves derived for the reference benchmark problem using the five models defined in Section 2.3 above and as specified in Table 5. Models 1 and 2 are the current Code methodology and the proposed modified Code methodology, respectively. In both of these cases, the flaw depth is 2.25" (t/4) and the K_I/K_{Ic} ratio is evaluated only at the deepest point of the flaw. The only loads included in models 1 and 2 are those produced by pressure and the through-wall thermal gradient. Models 1 and 2 include a safety factor of 2 on pressure loading. The minimum allowable pressure derived using model 1 is P_{CODE} = .43 ksi. The minimum allowable pressure derived using model 2 is $P_{NEWCODE}$ = 0.53 ksi.

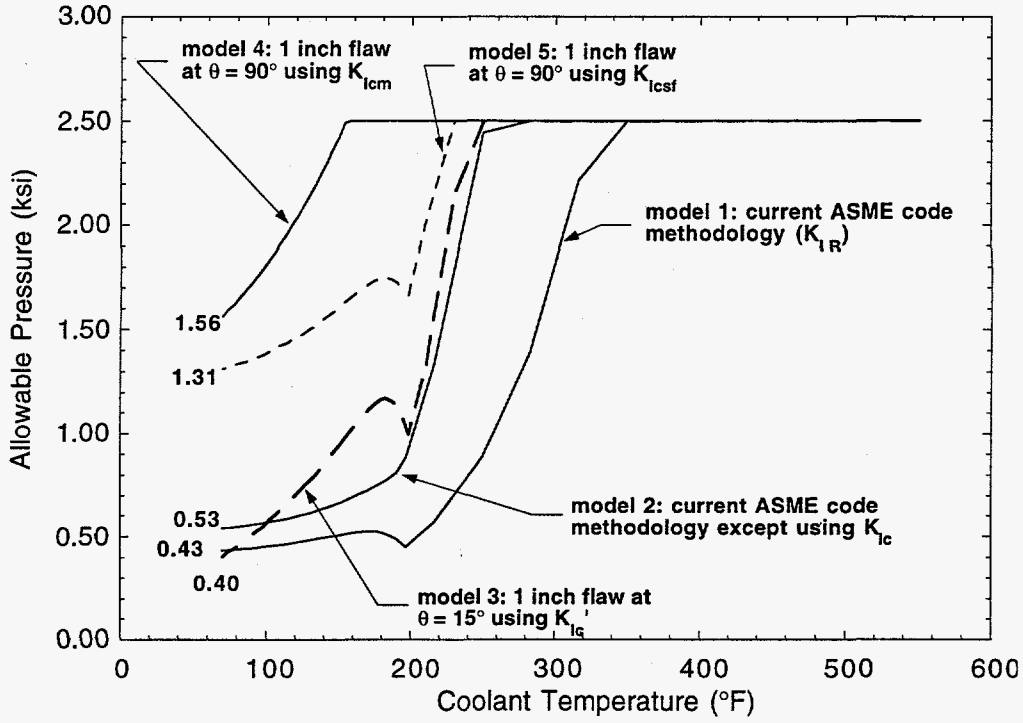

Fig. 17 Allowable pressure curves for 5 fracture models in Table 2 subjected to benchmark transient in Fig. 14.

Models 3-5 utilize the 1"deep flaw illustrated in fig. 15, the stress intensity factors illustrated in fig.16 and a safety factor of 1.0 on pressure loading. The only difference in models 3-5 is the representation of the fracture toughness. In each of these models, the entire crack front from the clad-base interface to the deepest point is considered.

Model 3, which applies the lower-bound curve to the EPRI K_{Ic} database (from which the ASME K_{Ic} curve was derived) in the region of interest [-200 °F ≤ (T-RT_{NDT}) ≤-150 °F], has a minimum best estimate (P_{BE}) pressure of 0.40 ksi.

Model 4, which applies the mean curve to the EPRI K_{Ic} database has a minimum best estimate (P_{BE}) pressure of 1.56 ksi. Results from this analysis, which utilizes a mean K_{Ic} curve in a deterministic

analysis, are provided for comparative purposes only. Use of a mean curve was not, per se, within the stated objective of this paper which was to compare fracture margins from best-estimate analyses with those derived from the current and proposed Code methodology, both of which use lower-bound (K_{Ia} and K_{Ic}) curves.

Model 5, which applies the lower-bound curve to the shallow flaw K_{JC} database for RPV materials, (see figure 4), has a minimum best estimate (P_{BE}) pressure of 1.31 ksi. A summary of results from each of the five cases evaluated in this study is given in Table 5.

Figure 18 shows the allowable pressure as a function of crack front angular location for models 3-5 at a transient time of 600 minutes, which is the time that the coolant reaches the ambient temperature and is also the time at which the lowest allowable pressure occurs. For model 3, the lowest allowable pressure on the crack front occurs at the clad-base interface whereas for models 4 and 5, the lowest allowable pressure occurs at the deepest point on the crack front.

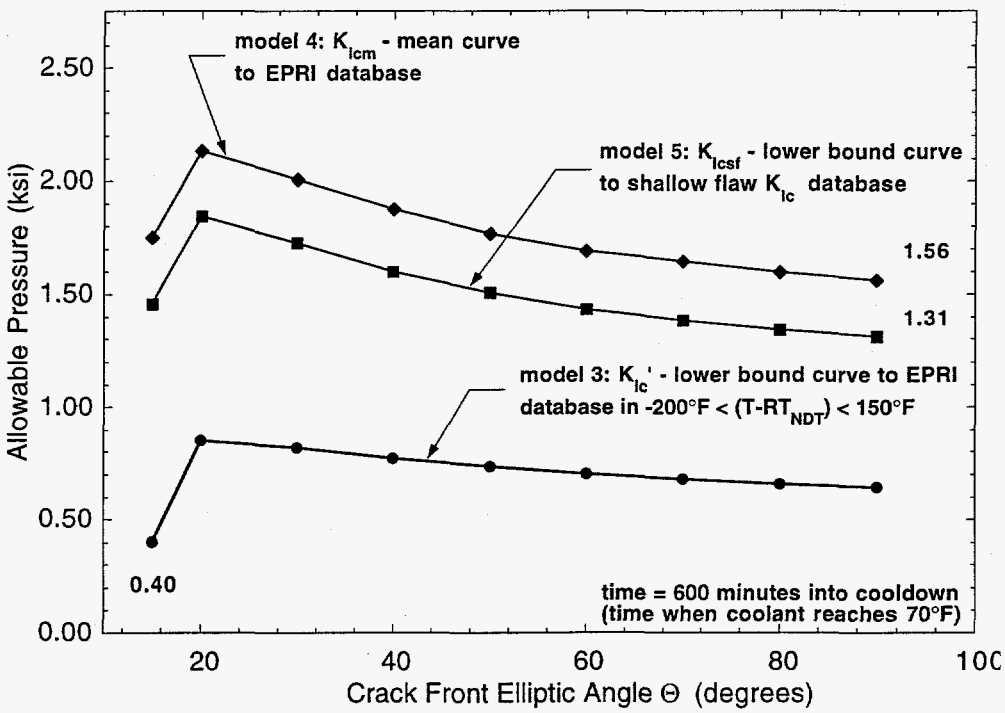

Fig. 18 Allowable pressure as a function of θ for reference benchmark problem at time = 600 minutes for three different representations of K_{Ic}.

As shown in fig. 17, the proposed change to the ASME code to replace the K_{Ia} curve with the K_{Ic} curve accomplishes the desired objective of opening-up the P-T operating envelope. The minimum allowable pressure for the benchmark problem is increased from the P_{CODE} value of 0.43 ksi to a $P_{NEWCODE}$ value of 0.53 ksi at the lowest coolant temperature. The increase in allowable pressure is larger at higher coolant

temperatures. The P_{BE} result from Case 5 of this study shows that adequate margins against brittle fracture of the RPV will be maintained if K_{Ia} is replaced by K_{Ic} in the ASME code P-T curve analysis procedure.

Table 5
Minimum Best Estimate Allowable Pressures (P_{BE}) for the Five Sample Problems

Case Number And Description	Flaw Geometry	Fracture Toughness	Loading	Safety Factor on Pressure	Allowable Pressure P_{BE} ksi
1. ASME Sect. XI, Appendix G	1/4T 6:1 surface, deepest point	K_{IR}	P+T	2	0.43
2. As (1) but with K_{Ic} replacing K_{Ia}	1/4T 6:1 surface, deepest point	ASME K_{Ic}	P+T	2	0.53
3. All loading plus SF=1 plus lower bound K_{Ic}'	a=1" 6:1 surface, deepest point & near clad	Lower-bound to the EPRI K_{Ic} data (K_{Ic}')	P+T+R+C	1	0.40
4. As (3) but with K_{Icm} replacing K_{Ic}'.	a=1" 6:1 surface, deepest point & near clad	Mean curve through the EPRI K_{Ic} data (K_{Icm})	P+T+R+C	1	1.56
5. As (3) but with shallow-flaw fracture toughness K_{Jcsf} replacing K_{Ic}'	a=1" 6:1 surface, deepest point & near clad	Lower-bound to the ORNL/David Taylor K_{Jcsf} data	P+T+R+C	1	1.31

P = Pressure, T = Thermal gradient, R = Residual stress in the structural weld, and C = clad-base material differential thermal expansion

6. Interim Conclusions

- Justification for changing the fracture toughness used in the ASME P-T curve analysis procedure from K_{Ia} to K_{Ic} requires a demonstration that $P_{BE} \geq P_{NEWCODE}$.
- $P_{BE} \geq P_{NEWCODE}$ has been demonstrated using the lower-bound to the shallow-flaw uniaxial- and biaxial-loading fracture toughness database for RPV materials.
- It is important to recognize that lower-bound to the shallow-flaw fracture toughness database is controlled by results from clad cruciform biaxial-loading tests conducted at normalized temperatures ($T-RT_{NDT}$) not less than -40°F. A potential exists for the estimated shallow-flaw

lower-bound fracture toughness to be further adjusted if data from clad cruciform biaxial-loading tests become available for the normalized temperature range -200°F ≤ T-RT_{NDT} ≤ 170°F.

- A preliminary evaluation of the stability of a sub-clad version of the reference flaw indicates that the irradiated cladding over the flaw may be breached by the ductile tearing, thereby converting the subclad flaw to a surface flaw. The P-T curve margin assessment should, therefore, be based on a surface-breaking flaw.

7. References

1. ASME Boiler and Pressure Vessel Code, Section XI, Appendix G, "Fracture Toughness Criteria for Protection Against Failure," New York, 1998.

2. USNRC Standard Review Plan, Overpressure Protection, NUREG-0800, Section 5.2.2, Rev. 3, Washington, DC, 1998.

3. Electric Power Research Institute, "White Paper on Reactor Vessel Integrity Requirements for Level A and B Conditions," EPRI TR- 100251, prepared by the Section XI Task Group on Reactor Vessel Integrity Requirements for the ASME Section XI Working Group on Operating Plant Criteria, Palo Alto, CA, January 1993.

4. R. K. Nanstad, et al., Oak Ridge National Laboratory, "Irradiation Effects on the Fracture Toughness of Two High-Copper Submerged-Arc Welds," HSSI Series 5, NUREG/CR-5913, Vol. 1, (ORNL/TM-122156/V1), October 1992.

5. Marshall, W., "An Assessment of the Integrity of PWR Pressure Vessels," report by a study group, United Kingdom Atomic Energy Authority, Harwell, Oxfordshire, United Kingdom, October 1, 1976.

6. S. R. Doctor, S. J. Schuster, and F. A. Simonen, Pacific Northwest National Laboratory, "Fabrication Flaws in Reactor Pressure Vessels," to be presented at the 26th Nuclear Regulatory Commission, Office of Nuclear Regulatory Research, Water Reactor Safety Meeting, at the Bethesda Mariott Hotel, October 26-28, 1998.

7. R. K. Nanstad, J. A. Keeney, and D. E. McCabe, "Preliminary Review of the Bases for the K_{Ic} Curve in the ASME Code," ORNL/NRC/LTR/93-15, July 12, 1993.

8. T. J. Theiss, et al., "Experimental and Analytical Investigation of the Shallow-Flaw Effect in Reactor Pressure Vessels," NUREG/CR-5886 (ORNL/TM-12115), July 1992.

9. W. J. McAfee, et al., "Biaxial Loading Effects on Fracture Toughness of Reactor Pressure Vessel Steel," NUREG/CR-6273 (ORNL/TM-12866), March 1995.

10. W. J. McAfee, et al., "Development of a Methodology for the Assessment of Shallow-Flaw Fracture in Nuclear Reactor Pressure Vessels: Generation of Biaxial Shallow-Flaw Fracture Toughness Data," ORNL/NRC/LTR-97/4, July 1998.

11. J. A. Keeney, et al., "Preliminary Assessment of the Fracture Behavior of Weld Material in Full-Thickness Clad Beams," NUREG/CR-6228 (ORNL/TM-12735), October 1994.

12. A. Keeney, et al., "Assessment of the Fracture Behavior of Weld Material in Full-Thickness Clad Beams," NUREG/CR-6380 (ORNL/TM-13091), in publication.

13. R. E. Link and J. A. Joyce, Naval Surface Warfare Center and U.S. Naval Academy, "Application of Fracture Toughness Scaling Models to the Ductile-to-Brittle Transition," NUREG/CR-6279, January 1996.

14. W. R. Corwin, W. E. Pennell, and J. V. Pace, Oak Ridge National Laboratory, "Reactor Pressure Vessel Integrity Research at the Oak Ridge National Laboratory," Proceedings of the U. S. Nuclear Regulatory Commission Twenty-Third Water Reactor Safety Meeting, NUREG/CP-0149, Vol. 3, March 1996.

15. W. J. McAfee, J. W. Bryson, R. D. Cheverton, and G. C. Robinson, "A Specimen and Method for Evaluating the Effect of Cladding on the Behavior of Subclad Flaws," PVP –Vol. 213/MPC-Vol. 32, Pressure Vessel Integrity, ASME, 1991.

16. F. M. Haggag et al., "Irradiation Effects on Strength and Toughness of Three-Wire Series-Arc Stainless Steel Weld Overlay Cladding," NUREG/CR-5511, (ORNL/TM-11439), February 1990.

17. T.L. Dickson, *FAVOR:* "A Fracture Analysis Code for Nuclear Reactor Pressure Vessels, Release 9401," ORNL/NRC/LTR 94-1, Martin Marietta Energy Systems, Inc., Oak Ridge National Laboratory, February 1994.

18. J.W. Bryson and T.L. Dickson, "Stress Intensity Factor Influence Coefficients for Axial and Circumferential Flaws In Reactor Pressure Vessels", Martin Marietta Energy Systems Inc., Oak Ridge National Laboratory, Pressure Vessel Integrity, PVP-Vol. 250, pp 77-88, ASME 1993.

19. J.W.Bryson and T.L. Dickson, Martin Marietta Energy Systems, Inc., Oak Ridge National Laboratory, "Stress-Intensity-Factor Influence Coefficients for Circumferentially Oriented Semielliptical Inner-Surface Flaws in Clad Vessels (Ri / t=10)," ORNL/NRC/LTR-94/8, April 1994.

20. J.A. Keeney and T.L. Dickson, Martin Marietta Energy Systems, Inc., Oak Ridge National Laboratory, "Stress-Intensity-Factor Influence Coefficients for Axially Oriented Semielliptical Inner-Surface Flaws in Clad Vessels (Ri / t =10)," ORNL/NRC/LTR-93/33- Revision 1, September, 1995.

21. ABAQUS User Manual, Hibbitt, Karlsson & Sorenson, Inc., Providence, Rhode Island (1995).

22. T.L. Dickson, "Validation of FAVOR Code Linear Elastic Fracture Solutions for Finite-Length Flaw Geometries," PVP-Vol. 304, Fatigue and Fracture Mechanics in Pressure Vessels and Piping, ASME 1995.

23. T. L. Dickson, et al., "The Inclusion of Weld Residual Stress In Fracture Margin Assessments of Embrittled Nuclear Reactor Pressure Vessels," PVP-Vol. 373, Fatigue, Fracture, and Residual Stresses, ASME 1998.